

---

# PERSISTENT TOPOLOGICAL FEATURES IN LARGE LANGUAGE MODELS

---

Yuri Gardinazzi<sup>1,2,\*</sup>, Giada Panerai<sup>1\*</sup>, Karthik Viswanathan<sup>3,1\*</sup>,

Alessio Ansuini<sup>1</sup>, Alberto Cazzaniga<sup>1</sup> and Matteo Biagetti<sup>1†</sup>

<sup>1</sup>Area Science Park, Trieste, Italy

<sup>2</sup>University of Trieste, Trieste, Italy

<sup>3</sup>University of Amsterdam, Amsterdam, the Netherlands

October 16, 2024

## ABSTRACT

Understanding the decision-making processes of large language models (LLMs) is critical given their widespread applications. Towards this goal, describing the topological and geometrical properties of internal representations has recently provided valuable insights. For a more comprehensive characterization of these inherently complex spaces, we present a novel framework based on zigzag persistence, a method in topological data analysis (TDA) well-suited for describing data undergoing dynamic transformations across layers. Within this framework, we introduce persistence similarity, a new metric that quantifies the persistence and transformation of topological features such as  $p$ -cycles throughout the model layers. Unlike traditional similarity measures, our approach captures the entire evolutionary trajectory of these features, providing deeper insights into the internal workings of LLMs. As a practical application, we leverage persistence similarity to identify and prune redundant layers, demonstrating comparable performance to state-of-the-art methods across several benchmark datasets. Additionally, our analysis reveals consistent topological behaviors across various models and hyperparameter settings, suggesting a universal structure in LLM internal representations.

## 1 Introduction

Large Language Models (LLMs) have revolutionized natural language processing by achieving unprecedented performance levels across a wide range of tasks (see [1] for a review). Despite their success, the black-box nature of these models has raised significant concerns about interpretability and transparency [2]. Moreover, their large scale demands a considerable amount of computational resources [3, 4], making it essential to reduce their size without compromising performance [5, 6, 7].

One strategy for addressing these issues has been to study the models' internal representations. Early works [8] demonstrated that visualization techniques can effectively uncover hierarchical representations within convolutional neural networks, highlighting how lower layers focus on edge detection while higher layers correspond to object parts and semantic concepts. Additionally, [9] illustrated that analyzing weight matrices and neuron activations can reveal interpretable features and organizational structures within deep networks, providing insights into how complex patterns are encoded and processed.

More recently, geometric studies made progress by introducing concepts like intrinsic dimension to characterize the manifold of internal representations and its evolution across layers [10, 11, 12]. These methods have been successfully applied to transformer models in various works [13, 14, 15]. One notable achievement of this approach has been to

---

\*These authors contributed equally to this work.

†Correspondence: [matteo.biagetti@areasciencepark.it](mailto:matteo.biagetti@areasciencepark.it)

show the emergence of semantic knowledge and abstraction phases in the middle layers of models, rather than at the final layers, as might be intuitively expected. However, these approaches provide only a static view of internal representations and suffer limitations in tracking their changes across layers.

A natural framework to address these limitations and to offer a more comprehensive characterization of the geometry of internal representations of neural networks is Topological Data Analysis (TDA). TDA is a set of unsupervised techniques that offers robust methods to describe the shape and structure of complex datasets. It has seen exponential growth with applications in computational biology [16], cosmology [17, 18]], personalized medicine [19], time-dependent data analysis [20], and machine learning [21], just to name a few. One prominent tool within TDA is persistent homology, which tracks the birth and death of topological features across different scales, thereby capturing the multiscale behavior of a point cloud. Several studies have proposed persistent homology to investigate neural networks and their internal representations (e.g. [22], [23, 24]).

However, in the context of TDA applications, it has not yet been recognized that the internal representations of LLMs can essentially be viewed as dynamic point clouds evolving in time (layers). As pre-trained LLMs process inputs, they transform these point clouds within the representation space layer by layer, capturing essential features and relationships throughout the model’s depth. Thus, it is natural to interpret these transformations as an evolving discrete dynamical system. TDA offers a specific framework for sequences of point clouds, known as *zigzag persistence*, built to characterize time-varying point clouds and temporal networks.

Following these ideas, we build a new framework based on zigzag persistence to analyse internal representations in LLMs by characterizing the birth and death of topological features within the model’s layers. Our zigzag algorithm achieves the following results:

- **Persistence Similarity:** We propose a new metric to measure which topological features persist across the layers of an LLM. Different than other similarity measures, persistence similarity tracks the entire trajectory of transformations between two layers.
- **Model Pruning:** By identifying layers with high persistence similarity, we prune redundant layers without significantly degrading performance, finding comparable results to state-of-the-art methods.
- **Consistency Across Models and Hyperparameters:** Our findings indicate that the behavior of persistent topological features and their similarities are consistent across different models, layers, and choices of hyperparameters of the framework. This consistency suggests a degree of universality in the topological structure of LLM representations.

In summary, our framework presents a novel perspective by combining two fundamental elements: firstly, it provides a fine-grained geometric analysis of the internal representations through TDA; secondly, the zigzag persistence framework tracks the trajectory of topological features across layers. Distinct from traditional methods that solely compare representations at individual layers, our approach captures their entire evolutionary path, providing a richer understanding of how these features evolve and contribute to the model’s decision-making processes.

## 2 Related Work

### Geometry and Topology of Internal Representations.

The manifold hypothesis suggests that high-dimensional data often lies on a lower-dimensional manifold [25]. The estimation of this approximated manifold, known as intrinsic dimension, changes dynamically in deep networks, expanding and contracting in ways that impact performance [10], learnability [12], and the network’s ability to generate flexible abstract data representations used for downstream tasks [11], [13]. Intrinsic dimension and neighbor composition analysis of internal representations of causal and masked transformer models helped in the localization of semantic information, and to highlight differences between real and artificial data [13, 14, 15]. Another approach to study the internal representation is to use topological methods of TDA. Studies on Convolutional Neural Networks (CNN) used topological descriptors to explore the shape of activation functions [26] or their relations to performance [23]. [24] introduced persistent homology dimension as an estimator of the intrinsic dimension of internal representations in CNNs, while [27] proposed a measure of similarity based on topological descriptors to compare representations. Betti numbers have been observed to remain stable across different datasets for the same architectures and to decrease as depth increases [28].

**Zigzag Persistence.** Zigzag persistence was introduced in [29, 30, 31] as an extension of persistent homology to study the persistence of topological features across sequences of spaces. This approach is particularly useful when data undergo dynamic changes or transformations over time. Since its introduction, zigzag persistence has been applied in various fields, including Hopf bifurcations in dynamical systems [32], commuting patterns in Great Britain’s

transportation network [33], coral reef ecosystems [34], cell location time series [35, 36], and honeybee aggregations [37]. It has also inspired methodological extensions such as multidimensional persistence [38] and the development of formigrams and crocker stacks [39].

**Layer Pruning by Similarity in Large Language Models.** Among existing methods to reduce the size of neural networks, layer pruning has gained particular relevance in the context of LLMs. The first applications to BERT models [40, 41, 42, 43] inspired a long series of experiments employing similar techniques [44, 45, 46, 47, 48, 49]. Many of these efforts base their methodology on similarity measures of internal representations, which have conveniently been summarized in a recent review [50]. In this work, we consider [6], which uses angular similarity, and [7], which uses Block-Influence similarity, as a reference point for comparison.

### 3 Method

In this section, we introduce the zigzag persistence framework, which we use to analyze the internal representations of LLMs pre-trained with an autoregressive loss. These models typically receive an input sequence of  $n$  tokens (often representing a sentence) embedded in a  $d$ -dimensional space. The input is transformed across the layers of the network without altering the embedding dimension. Due to the autoregressive nature of these models, the representation of the last token in a sequence captures information about the entire sequence and is the only token used for predicting the next. As a result, we choose to focus on the final token representation at each layer when analyzing input sequences. Thus, our data points in the representation space are vectors in a  $d$ -dimensional space,  $\{\mathbf{x}_i(\ell_j)\} \in \mathbb{R}^d$ , for  $i = 1, \dots, N_{\text{sentences}}$  and  $j = 1, \dots, N_{\text{layers}}$ , with each vector representing a sentence at a specific layer. Drawing from applications of topological data analysis, and particularly zigzag persistence in similar contexts, we interpret each layer as a snapshot of a complex, high-dimensional, time-varying system evolving through different stages (layers).

#### 3.1 Topological Data Analysis and Persistent Homology

Topological data analysis [51, 52] provides a tool for geometrically characterizing highly complex datasets. Within this framework, persistent homology [53] is the key methodology to characterize a point cloud on multiple scales at once. Its goal is to identify the range of scales over which a particular class of topological features (connected components, loops, voids, higher dimensional “holes”) remain relevant, or “persistent”, as opposed to “topological noise”, i.e. features disappearing roughly at the same scale they formed. The basic ingredients for this technique are i) a criterion to connect points, forming a *simplicial complex* and ii) a scale parameter  $\nu$  (often a coarsening scale) such that given  $\nu_1 \leq \nu_2$ , then the two corresponding simplicial complexes are related by  $K_{\nu_1} \subseteq K_{\nu_2}$ . The ordered sequence of simplicial complexes for varying scale parameters is called *filtration*. An intuitive example is the Vietoris-Rips filtration, built from complexes parametrized by the radius of the ball drawn around each point of the dataset.

Filtrations can be generalized to a more flexible structure called a *zigzag filtration*. Unlike a standard filtration, a zigzag filtration allows the sequence of complexes to move both forward and backward, meaning that inclusions between complexes can reverse at certain steps. We take this approach in our study to track the evolution of the internal representations *across* layers, rather than at a fixed snapshot, as done in traditional persistent homology implementations. In this sense, our parameter is not a distance/coarsening scale, but a discrete *time* scale represented by the layer number. We track topological features as they are formed and destroyed along the layers of the model and we statistically characterize these changes to describe a complex series of transformations in high-dimensional space. Differently than standard persistent homology, short- and long-lived features represent how the model dynamically evolves. Short-lived features indicate a high rate of rearrangement of the points  $x_i$  between adjacent layers, while long-lived features suggest a phase of retention of (relative) positions in the model. This is a crucial point in our analysis, as it provides a novel tool to geometrically interpret the model’s internal representations. We now outline the main steps of the zigzag algorithm, leaving a rigorous mathematical formulation to Appendix A.

#### 3.2 The zigzag algorithm

We aim to study internal representations by tracking statistical changes in the formation of  $p$ -dimensional holes, or  $p$ -cycles, generated by connecting nearby data points within each layer  $\ell_i$ . As introduced above, the first ingredient for a TDA formulation is a criterion for connecting points of the dataset. In this regard, we construct a  $k$ -Nearest Neighbors graph  $G_{\ell_i} = (V_{\ell_i}, E_{\ell_i})$  at every layer  $\ell_i$ , where the number  $k_{\text{NN}}$  of neighbors is a fixed hyperparameter. To exploit the knowledge that the manifold on which the data lie is typically much smaller than the high-dimensional ambient space, we extend the dimension of the graph by filling higher-dimensional simplices. More precisely, we *fill* a simplex when its boundary, composed of lower-dimensional simplices (such as vertices and edges), is complete. In particular, we consider a triangle as filled when it has three vertices with pairwise connections. Similarly, a tetrahedron is filled

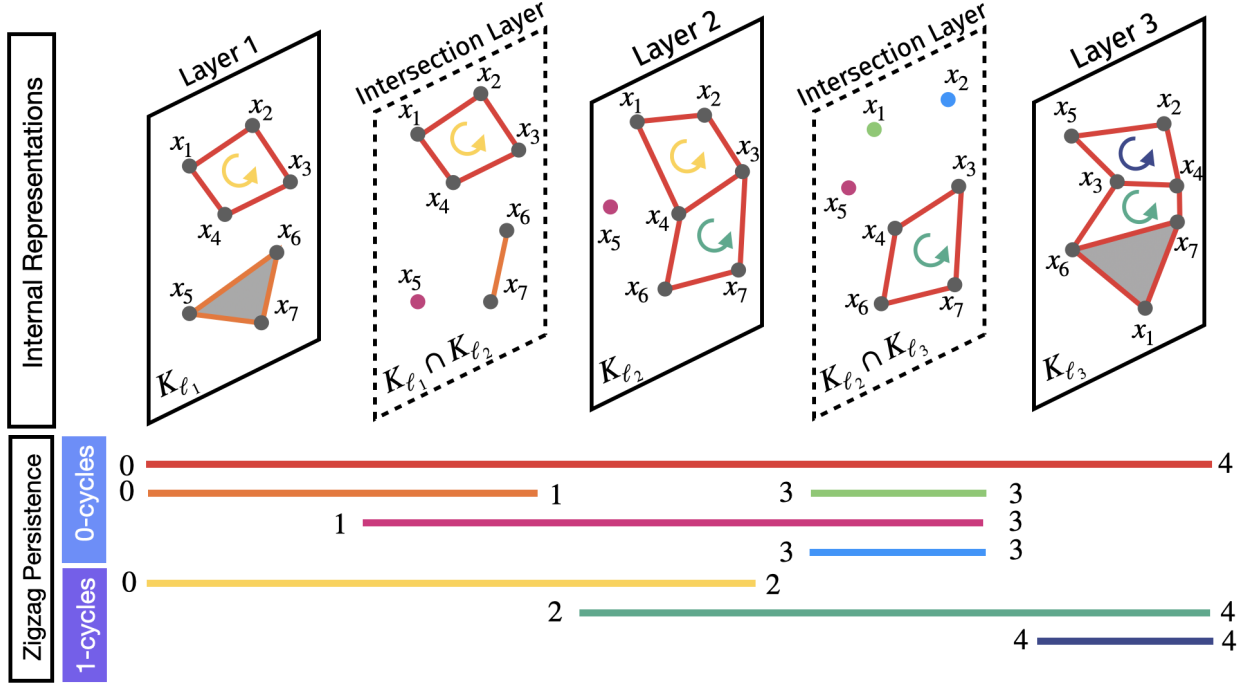


Figure 1: A schematic representation of the zigzag algorithm.

when four vertices are all interconnected by edges, totaling six edges. This concept extends to higher dimensions up to a specified maximum dimension  $m$ . Thus, in each layer, we construct the simplicial complex  $K_{\ell_i}$  defined by:

$$K_{\ell_i} = \bigcup_{S \subseteq V_{\ell_i}} \{S \mid \forall x_s, x_l \in S, (x_s, x_l) \in E_{\ell_i} \text{ and } |S| \leq m + 1\}. \quad (1)$$

To track changes in the network, we compute intersection layers by identifying simplices present simultaneously in both adjacent layers. This allows us to construct a sequence of inclusions between these complexes

$$\begin{array}{ccccccc} K_{\ell_1} & & K_{\ell_2} & & K_{\ell_{L-1}} & & K_{\ell_L} \\ & \swarrow & & \swarrow & & \swarrow & \\ & K_{\ell_1} \cap K_{\ell_2} & & \dots & & K_{\ell_{L-1}} \cap K_{\ell_L} & \end{array} \quad (2)$$

where we define  $L \equiv N_{\text{layers}}$  for conciseness. This sequence represents our zigzag filtration, denoted by  $\Phi$ . This filtration is the second ingredient needed to define persistent homology. We thus define a notion of *birth* and *death* of  $p$ -dimensional topological features, also denoted as  $p$ -cycles, with  $p = 0, \dots, m - 1$ , being  $m$  the maximum dimension at which we expand the graph. Throughout this work, we choose  $m = 4$ , which implies that the  $p$ -cycles are well defined up to dimension  $p = 3$ . These cycles can be thought of as holes in their respective dimension. We can track the persistence of these cycles as they appear in a given layer when a group of points exhibits a particular proximity and distribution in the complex and disappear at a subsequent layer when some points have moved apart, causing the cycle to vanish. We illustrate the idea in Figure 1. The output of the zigzag algorithm is then a multiset of birth-death pairs [birth, death]<sup>3</sup>, known as the *persistence diagram*

$$\text{Pers}_p(\Phi) = \left\{ [\text{birth}, \text{death}] \mid \text{birth}, \text{death} \in \{0, \dots, 2N_{\text{layers}} - 1\} \right\}. \quad (3)$$

We thus work with a zigzag filtration naturally indexed by  $\{0, 1, 2, \dots, 2N_{\text{layers}} - 1\}$ . Specifically, as shown in the Figure 1, even numbers starting from 0 are assigned to  $p$ -cycles that emerge and disappear within the model layers. In contrast, odd numbers are designated for features at the intersection layers. It is important to note that  $p$ -cycles

<sup>3</sup>The repetition of a pair [birth, death] indicates that multiple cycles in dimension  $p$  have been created and destroyed in correspondence of the same layers.

are defined as equivalence classes, meaning that a cycle need not maintain the same form at the level of simplices throughout its lifetime. The orange 0-cycle in the figure exemplifies this: in Layer 1, the cycle corresponds to a filled triangle,  $\{x_5, x_6, x_7\}$ , but in the intersection layer, it is reduced to the edge  $\{x_6, x_7\}$ . In Layer 2 this edge merges with another 0-cycle (depicted in red), marking the death of the orange cycle. A mathematical explanation of this is provided in Appendix A. This feature ensures robustness of our construction to small changes in the  $k_{\text{NN}}$  graph. The corresponding algorithm that generates  $\text{Pers}_p(\Phi)$  is schematically described below.

---

**Algorithm 1** Zigzag algorithm
 

---

**Require:**  $model, dataset, k_{\text{NN}}, m$

$reps \leftarrow \text{extractRepresentations}(model, dataset)$

$K \leftarrow []$

**for**  $i \leftarrow 1$  to  $model.getNumLayers()$  **do**

$graph \leftarrow \text{kNearestNeighborsGraph}(reps[i], k_{\text{NN}})$

$K.append(\text{graphExpansion}(graph, m))$

**end for**

$K_{\text{int}} \leftarrow \text{computeIntersectionLayers}(K)$

$f, times \leftarrow \text{computeFiltrationTimes}(K, K_{\text{int}})$

$\Phi \leftarrow \text{FastZigZag}(f, times)$

---

It exploits two existing public codes that were developed for zigzag computations: DIONYSUS2 [54] and FASTZIGZAG [55]. DIONYSUS2 is a C++ library for computing persistent homology, with a specific library for zigzag persistence. In our case, it has the role of extracting the filtration  $f$  and computing the  $times$  array, i.e. the list of layer indices to be associated with the birth and death of the simplices across the filtration. FASTZIGZAG allows to calculate efficiently <sup>4</sup> the persistence diagram  $\text{Pers}_p(\Phi)$  by converting the input zigzag filtration to a non-zigzag filtration of an equivalent complex with the same length, and it then converts the obtained persistence intervals back to zigzag.

### 3.3 Effective Persistence Image

The pairs generated within  $\text{Pers}_p(\Phi)$  are best understood by visualizing them through a *persistence image*, a well-known descriptor within the TDA tools. The persistence image in our case results in a grid of size  $(2N_{\text{layers}} - 1) \times (2N_{\text{layers}} - 1)$ , for each homology dimension  $p$ . Each pixel in the grid is associated with an integer value corresponding to the number of cycles appearing with that birth-death pair. Defined this way, the persistence image does not discriminate between the model and intersection layers. Their behavior is generally fairly different, and have an alternating structure between model and intersection layers. Hence, persistence images are not *smooth* as a function of layers. To achieve a smoother representation, we introduce *effective persistence images*, obtained by excluding the intersection layers from the construction. This is achieved by defining a map, similar to the approach in [56], that translates the collection of intervals from the zigzag persistence diagram of the filtration in equation 2 into intervals, where the birth and death occur only across model layers. Formally, for  $b, d > 0$ , we obtain:

$$\widehat{PI}_p(b/2, d/2) = PI_p(b, d) + PI_p(b-1, d) + PI_p(b, d-1) + PI_p(b-1, d-1), \quad (4)$$

where  $\widehat{PI}_p$  is the effective persistence image for the  $p$ -cycles and  $b, d$  are model layers indexed by even numbers.<sup>5</sup>

The collection of  $\widehat{PI}_p$ s taken over all  $p$  contains all the information output from our zigzag algorithm, and give a useful overview of the model as a whole. On the other hand, they are not easily tractable in a statistical sense and hard to interpret. Indeed, one focus of this work is to look at the fine-grained topological structure of representation space, tracking the persistence of cycles across layers. For this purpose, we develop a suited summary of the effective persistence image in the next section.

---

<sup>4</sup>The algorithm performs well even for the relatively large datasets we employ for this analysis: with 10K points embedded in a space with dimension  $d = 4096$ , a number of neighbors for the  $k_{\text{NN}}$  graph of  $k_{\text{NN}} = 10$ , and a maximum homology dimension of  $m = 10$  on an AMD EPYC 7H12 it takes approximately 2 hours.

<sup>5</sup>Note that this operation does not modify the information about the model layers contained in the original  $\text{Pers}_p(\Phi)$ , as it redefines consistently all the births and deaths.

### 3.4 Persistence Similarity

Given two layers  $\ell_1, \ell_2$ , we define the *persistence similarity* as the fraction of  $p$ -cycles in  $\ell_1$  that exist in  $\ell_2$  as well, and have existed throughout the layers in between. Mathematically it can be expressed as

$$\mathcal{S}_p(\ell_1, \ell_2) = \frac{\sum_{\ell_1 \leq M_1, \ell_2 \geq M_2} \widehat{PI}_p(\ell_1, \ell_2)}{\beta_p(\ell_1)} \quad (5)$$

$$M_1 = \min(\ell_1, \ell_2); \quad M_2 = \max(\ell_1, \ell_2)$$

where  $\beta_p(\ell)$  is the Betti number, i.e. the number of alive  $p$ -cycles at layer  $\ell$ . Given a  $p$ -cycle that is alive at a given layer  $\ell$ , we can thus define the average probability of finding it alive at any other layer as

$$\bar{\mathcal{S}}_p(\ell) = \frac{1}{N_{\text{layers}}} \sum_{\ell_i=1}^{N_{\text{layers}}} \mathcal{S}_p(\ell, \ell_i), \quad (6)$$

which indicates the degree of ‘‘mobility’’ of the system at a given layer, i.e. overall retention of cycles in each model layer. Thus, a low value of  $\bar{\mathcal{S}}_p$  represents a phase during which internal representations are undergoing major topological changes, causing points of the dataset to change relative positions abruptly. For high values, the inverse is true, i.e. the relations among points are relatively stationary. It is worth noting that traditional measures of similarity between layers typically depend solely on their current state, namely the activation matrices on the set of data. In contrast, our method considers the trajectory from  $\ell_1$  to  $\ell_2$ , implying that persistence similarity does not just depend on the initial and final states but also on the path between them.

## 4 Experiments

### 4.1 Models, Datasets and Benchmarks

We work with 4 models: Llama2 [57], Llama3 [58], Mistral [59] and Pythia 6.9b [60]. These models are open-source decoder-only transformers, and they achieve high performance in the benchmarks we consider in this work. Llama2-7B, Llama3-8B, Mistral 7B, and Pythia 6.9b have 32 hidden layers, Llama2-13B has 40 hidden layers, and both Llama2-70b and Llama3-70b have 80 hidden layers.

For our purposes, the input dataset from which we take internal representations must provide a fair test of how the model processes and understands language. An extensive and accessible corpus is the Pile dataset [61], which combines 22 datasets over a wide range of topics and structures. For computational reasons, we take the Pile-10k subset, accessible on HuggingFace.<sup>6</sup> For completeness, we also consider the Stanford Sentiment Treebank (SST) dataset [62]. From these datasets, each prompt is processed so that the last token is extracted at each normalization layer and the final normalization applied to the output layer.

We use 3 benchmarks for layer pruning performance evaluation: MMLU [63], HellaSwag [64], and Winogrande [65], which have been widely used for similar purposes in previous analyses. The benchmarks are evaluated for the models with the use of the library lm-eval-harness by [66] with a 5-shot setup.

### 4.2 Zigzag persistence applied to LLM models

**Effective Persistence Image.** We generate an effective persistence image for each model using the two datasets, each homology dimension up to  $p = 3$ , and for a range of values of  $k_{\text{NN}} \in [1, 15]$ . We show an example of this effective persistent image in Figure 2 for the Llama 3 8B model for the SST dataset for 1- and 2- cycles for  $k_{\text{NN}} = 5$  and  $k_{\text{NN}} = 15$ , respectively.<sup>7</sup> The choice of the hyperparameter  $k_{\text{NN}}$  is done so as to maximize the total number of cycles. The x-axis represents the layer at which a  $p$ -cycle is born, and the y-axis represents persistence, i.e. death layer - birth layer. The colorbar measures the amount of  $p$ -cycles on a given grid point. As expected, a large number of cycles are very short lived, i.e. the grid points at persistence equal unity. On the other hand, we observe that persistence is typically higher for  $p$ -cycles born after the first half of the model’s depth, a feature that is visually evident on the right panel of Figure 2, representing 2-cycles, but observed across all models and dimensions, especially for 1-cycles. A fraction of these cycles have maximal persistence, i.e. they survive until the last layer.

<sup>6</sup><https://huggingface.co/datasets/NeelNanda/pile-10k>

<sup>7</sup>The reason for using the SST dataset, instead of Pile, is that the 70B models are computationally expensive for the latter. We show that results are consistent in Appendix C.

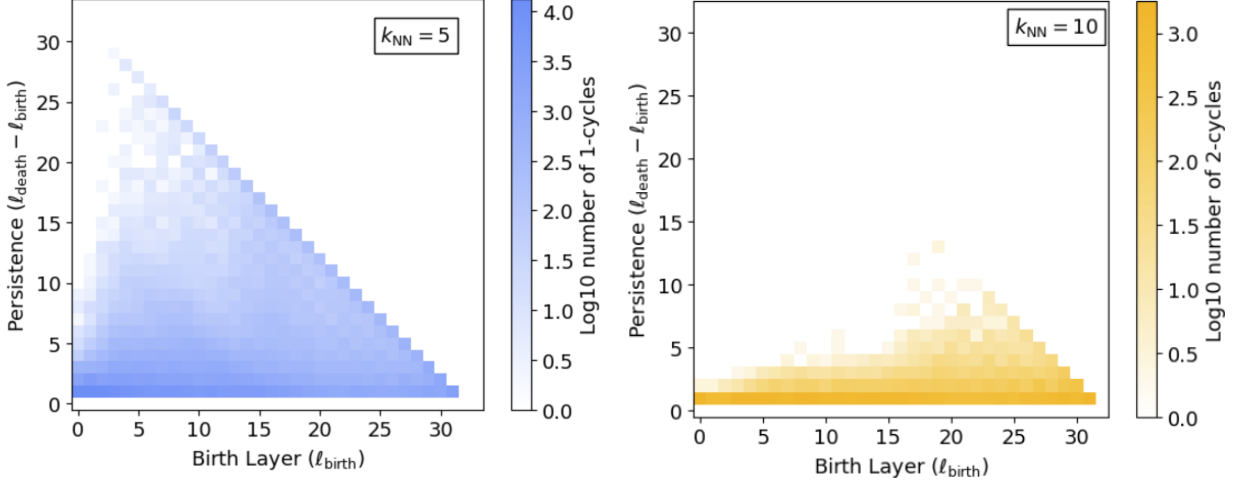


Figure 2: Effective persistence image for the Llama 3 8B model using the SST dataset. We show 1-cycles (Left Panel) and 2-cycles (Right panel). The corresponding  $k_{NN}$  graph is constructed with  $k_{NN} = 5$  and  $k_{NN} = 10$ , respectively. The density plot shows the amount of cycles (colorbar) for a given birth-persistence pair (x- and y-axis), where values refer to the model layer.

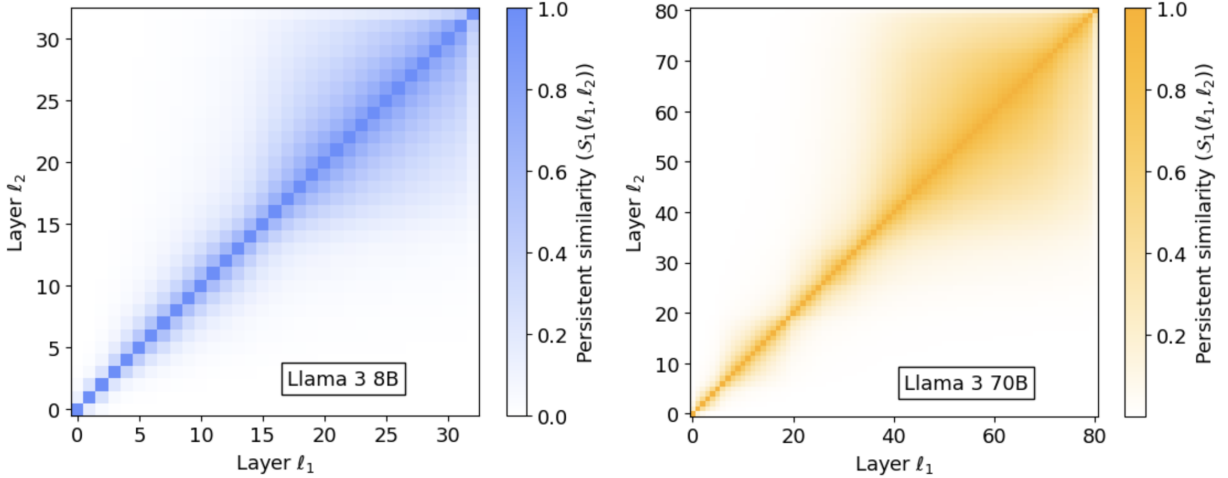


Figure 3: Persistence similarity of 1-cycles as defined in equation 5 for Llama 3 of two different sizes (8B and 70B) and the SST dataset. For both models we fix  $k_{NN} = 5$ . A given pixel of the grid represents similarity computed between two layers. Darker regions indicate higher similarity.

In computing  $\widehat{PI}_p$ s across models, dimensions and  $k_{NN}$  values, we observe that 0- and 3-cycles are relatively low in number, while 1- and 2-cycles are higher, reaching tens of thousands of cycles per layer. This behaviour might be expected for a  $k_{NN}$ -graph based construction, since connections are dense even for low values of  $k_{NN}$ , especially if points are concentrated in low dimensional regions of the representation space. We examine this behavior in detail to make sure that our construction is stable for different choices on the  $k_{NN}$  graph, see Appendix B for details.

The  $\widehat{PI}_p$ s from Figure 2 are suggestive of important features in the topology of internal representations, which we look at in more detail using persistence similarity. Given the prevalence of 1-cycles across various models, layers, and choices of  $k_{NN}$ , we concentrate on these features in the following discussion.

**Persistence similarity.** We can visualize persistence similarity, as defined in equation 5,  $S_1(\ell_1, \ell_2)$  as a density plot, shown in Figure 3 for Llama 3 of two different sizes (8B and 70B) and the SST dataset, with corresponding plots for Pile for the 8B shown in Appendix C. Again, we choose  $k_{NN} = 5$  although results are similar within the  $k_{NN} \in [1, 15]$  range. In these plots, darker regions indicate a higher fraction of  $p$ -cycles alive between two given layers. Note that

the plot is not symmetric by definition (cfr. equation 5) meaning that at a given layer, the fraction of cycles alive at an earlier layer might be different than the ones alive at a later layer. Nevertheless,  $\bar{\mathcal{S}}_p$  is approximately symmetric. Both models clearly show a high degree of similarity roughly midway through the depth, until before the last few layers. This is in agreement with what observed in the  $\bar{P}I_p$ , which suggested that a  $p$ -cycle born after the first half of the model is likely to survive until the last layer. We now compute the average similarity, i.e. the average over the

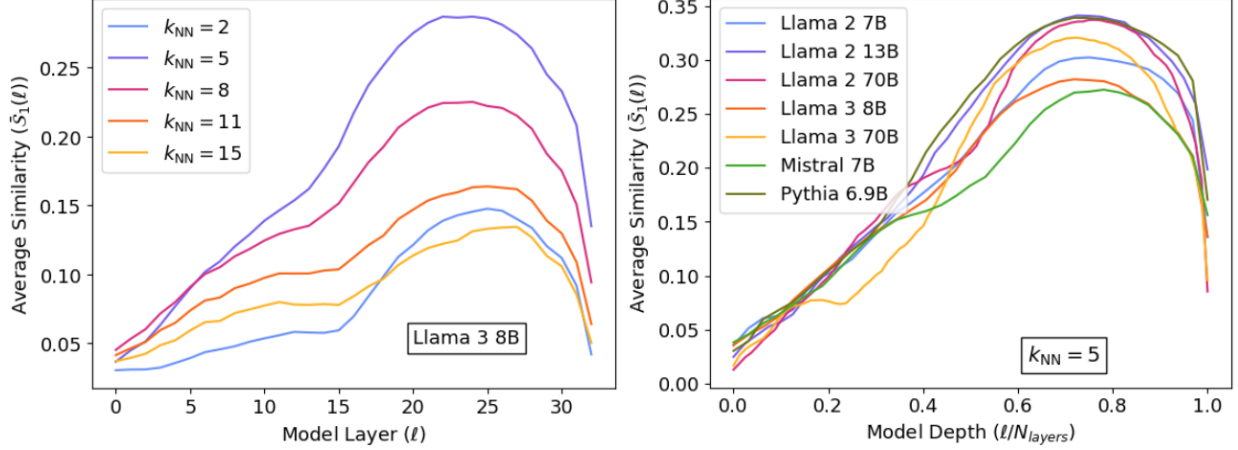


Figure 4: Average Similarity as a function of model depth, computed for Llama 3 8B and varying  $k_{NN}$  parameter (Left Panel) and at fixed  $k_{NN} = 5$  parameter and varying models (Right Panel).

column of persistence similarity (cfr. equation 6),  $\bar{\mathcal{S}}_p$  both at fixed model and varying  $k_{NN}$  parameter, and at fixed  $k_{NN}$  parameter and varying model, as a function of the model’s depth. Results are shown in the Left and Right Panels of Figure 4, respectively. Based on the Left Panel, we choose  $k_{NN} = 5$  as representative value for the Right Panel, given that it gives the highest values of  $\bar{\mathcal{S}}_1$ . Remarkably,  $\bar{\mathcal{S}}_1$  peaks at the same relative depth for a wide variety of models, while the parameter  $k_{NN}$  only changes the normalization of the curve. This result is in agreement with previous results finding that the fraction of similar layers is approximately universal across models (e.g. [6, 7]).

### 4.3 Layer pruning by persistence similarity

Recently, measures of layer similarity have been used to identify layers that contribute minimally to the performance of LLMs. These layers can be pruned, and the performance re-evaluated to validate this assumption. Since persistence similarity tracks changes across layers, it can be leveraged for layer pruning by selecting layers that retain the most cycles. Consequently, we establish a pruning criterion based on average persistence similarity  $\bar{\mathcal{S}}_1$  computed now on the Pile dataset. Specifically, we prune layers that lie within 10% and 20% of the maximum  $\bar{\mathcal{S}}_1$ , corresponding to conservative and aggressive pruning, respectively. Here is a schematic summary of the algorithm.

---

#### Algorithm 2 Pruning algorithm

---

**Require:**  $\bar{\mathcal{S}}_1, model, threshold,$   
 $max \leftarrow \max(\bar{\mathcal{S}}_1)$   
 $layersToRemove \leftarrow []$   
**for**  $l \leftarrow 1$  to  $model.getNumLayers()$  **do**  
    **if**  $\bar{\mathcal{S}}_1[l] > max * threshold$  **then**  
         $layersToRemove.append(l)$   
    **end if**  
**end for**  
 $model.removeLayers(layersToRemove)$

---

The algorithm outputs how many and which layers have high degree of persistence similarity. We now cut those layers and measure performance using the benchmarks introduced in Section 4 and across models considered in this work.

We compare to layer pruning methods based on state of the art measures of similarity, namely [6] and [7]. Both approaches are designed to take as input the desired number of layers to prune  $N_{prune}$  and measure performance as  $N_{prune}$  grows. For a fair comparison, we feed the number of layers cut by our method as an input to the other two



Models	MMLU			HellaSwag			WinoGrande		
	Full	This work	Other works	Full	This work	Other works	Full	This work	Other works
Llama 2 7B	45.74	37.38 (39.32)	<b>43.95</b> (34.35)	58.54	<b>44.71</b> (32.10)	42.78 (35.10)	74.43	<b>68.67</b> (59.67)	67.72 (62.67)
Llama 2 13B	54.60	50.16 (36.45)	<b>50.71</b> (37.91)	61.43	<b>48.60</b> (34.35)	47.84 (34.52)	76.72	71.67 (63.21)	<b>73.15</b> (61.47)
Llama 3 8B	65.07	<b>53.44</b> (23.16)	<b>53.44</b> (24.33)	61.37	<b>41.60</b> (29.69)	<b>41.60</b> (27.10)	77.10	<b>70.00</b> (59.75)	<b>70.00</b> (50.58)
Mistral 7B	62.40	<b>53.17</b> (24.26)	38.20 (37.86)	62.83	<b>36.67</b> (26.26)	34.45 (28.10)	77.35	<b>66.50</b> (57.76)	63.76 (55.96)
Pythia	-	-	-	49.70	31.43 (31.23)	<b>34.96</b> (26.84)	63.30	55.71 (54.84)	<b>58.09</b> (51.07)

Table 1: **Benchmark Table.** For each benchmark we show three columns: (i) *Full*, represents the accuracy of the model without any layer pruned. (ii) *This work*, accuracy of the model with two different cuts, at 10% and 20%, where layers are pruned following the algorithm 2). The results are in the form 10% cut (20% cut) (iii) *Other works*, accuracy obtained by considering the same amount of layer pruned estimated with our method and then computing the layer to be pruned with two different similarity measures: angular distance from [6] and Bi-score from [7]. The chosen layers turn out to be the same for the two methods, so the results are condensed in one column, and they are then represented in the format *first-block-cut(second-block-cut)*.

methods, and verify which layers they select to cut given this input, and the corresponding performance. We show a schematic diagram of the layers cut with our method (Bottom Row) and the other two methods (Upper Row) in Figure 5. Interestingly, both considered methods from [6] and [7] give the same result at fixed  $N_{\text{prune}}$ , thus we refer to them simply as “other works”.

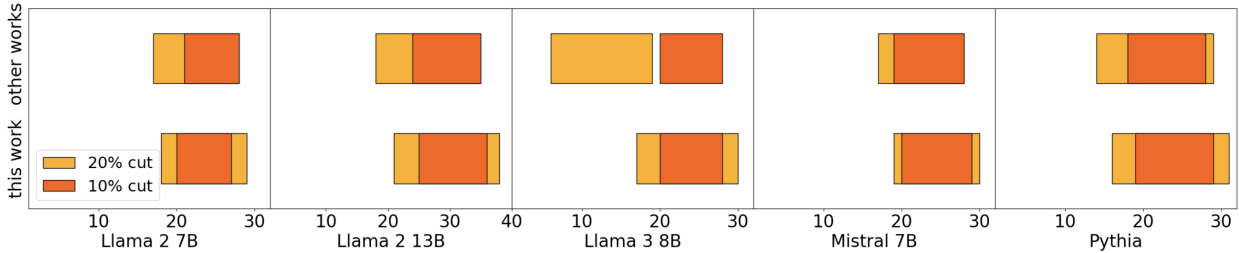


Figure 5: Pruned layers across models based on persistence similarity (Bottom Row) and other methods from [6, 7]. Since both these two methods give the same results, we generically call them “other works”. The number of layers pruned for all methods is defined by cutting layers that are within 10% (orange) and 20% (yellow) of the maximum average similarity,  $\bar{S}_1$ .

The 10% pruning is rather consistent across methods, with small variations. The more aggressive cut of 20% generates more discrepancies, especially for Llama 3 8B, where both methods from [6] and [7] prefer to cut earlier layers.

We now show performance results in Table 1,<sup>8</sup> where in bold we indicate the layer pruning method that has better or equal performance with respect to the other method. Despite often selecting different layers, our topology-based pruning strategy achieves generally comparable results to methods from [6] and [7], and it surpasses their result in approximately for half of the model-benchmark combinations.

## 5 Conclusions

In this work, we have introduced a novel framework for analyzing the internal representations of LLMs using zigzag persistence, a tool from TDA. Our approach aims to provide a high-level geometrical and topological description of

<sup>8</sup>Results for Pythia on MMLU tasks are not shown because the model is not designed for following the format of the tasks, as shown in [60].

positional and relational changes across layers. Our zigzag algorithm introduces a new metric, persistence similarity, which uniquely tracks the trajectory of topological features such as  $p$ -cycles across layers. This approach allows for effective model pruning by identifying and removing redundant layers without significantly compromising performance, yielding results comparable to state-of-the-art methods. Furthermore, our findings show that the behavior of persistent topological features and their similarities remain consistent across various models, layers, and hyperparameter settings, suggesting a universal topological structure in LLM representations. This work offers a new perspective by providing a finer-grained geometric analysis and a framework that accounts for the evolutionary path of topological features, enhancing both interpretability and efficiency of LLMs.

There are several limitations in our study that future research could address. First, while our method shows robustness across hyperparameters within the framework, these choices need not be optimal. Defining an appropriate criterion for connecting points in the representation space, and consequently, a filtration, is a delicate task in TDA that could require further investigations to detail the impact of the various choices on the construction of the filtration. Our topology-based pruning strategy gives strong results only considering two scenarios (cutting 10% and 20% based on average persistence similarity). Nevertheless, a more accurate approach could consider iteratively pruning until the best performance is reached with maximal reduction. Lastly, our study primarily focuses on static, pre-trained models. Extending this framework to track the evolution of internal representations during training would require computational optimization of the algorithm but could provide the opportunity to directly optimize model size using persistence similarity.

## Reproducibility

All the results contained in this work are reproducible by means of a repository that can be found at this link: <https://github.com/RitAreaSciencePark/ZigZagLLMs>.

## Acknowledgments

We thank Mathieu Carrière and Magnus Botnan for helpful discussions on the TDA implementation and suggestions on the zigzag algorithm. M.B., Y.G. and G.P. are supported by the Programma Nazionale della Ricerca (PNR) grant J95F21002830001 with title “FAIR-by-design”. K.V. was partially supported by Programma Nazionale della Ricerca (PNR) grant J95F21002830001 with the title “FAIR-by-design” during his visit to Area Science Park while this project was in its development phase. A.A. and A.C. were supported by the project “Supporto alla diagnosi di malattie rare tramite l’intelligenza artificiale” CUP: F53C22001770002. A.A. and A. C. were supported by the European Union – NextGenerationEU within the project PNRR “PRP@CERIC” IR0000028 - Mission 4 Component 2 Investment 3.1 Action 3.1.1.

We thank Area Science Park supercomputing platform ORFEO made available for conducting the research reported in this paper and the technical support of the Laboratory of Data Engineering staff.

## References

- [1] M. A. K. Raiaan, M. S. H. Mukta, K. Fatema, N. M. Fahad, S. Sakib, M. M. J. Mim, J. Ahmad, M. E. Ali, and S. Azam, “A review on large language models: Architectures, applications, taxonomies, open issues and challenges,” *IEEE Access* **12** (2024) 26839–26874.
- [2] Q. V. Liao and J. W. Vaughan, “Ai transparency in the age of llms: A human-centered research roadmap,” 2023. <https://arxiv.org/abs/2306.01941>.
- [3] S. Samsi, D. Zhao, J. McDonald, B. Li, A. Michaleas, M. Jones, W. Bergeron, J. Kepner, D. Tiwari, and V. Gadepally, “From words to watts: Benchmarking the energy costs of large language model inference,” in *2023 IEEE High Performance Extreme Computing Conference (HPEC)*, pp. 1–9. 2023.
- [4] G. Bai, Z. Chai, C. Ling, S. Wang, J. Lu, N. Zhang, T. Shi, Z. Yu, M. Zhu, Y. Zhang, C. Yang, Y. Cheng, and L. Zhao, “Beyond efficiency: A systematic survey of resource-efficient large language models,” 2024.
- [5] X. Ma, G. Fang, and X. Wang, “LLM-pruner: On the structural pruning of large language models,” in *Thirty-seventh Conference on Neural Information Processing Systems*. 2023. <https://openreview.net/forum?id=J8Ajf9WfXP>.
- [6] A. Gromov, K. Tirumala, H. Shapourian, P. Glorioso, and D. A. Roberts, “The unreasonable ineffectiveness of the deeper layers,” 2024. <https://arxiv.org/abs/2403.17887>.
- [7] X. Men, M. Xu, Q. Zhang, B. Wang, H. Lin, Y. Lu, X. Han, and W. Chen, “Shortgpt: Layers in large language models are more redundant than you expect,” 2024. <https://arxiv.org/abs/2403.03853>.

- [8] M. D. Zeiler and R. Fergus, “Visualizing and understanding convolutional networks,” in *Computer Vision – ECCV 2014*, D. Fleet, T. Pajdla, B. Schiele, and T. Tuytelaars, eds., pp. 818–833. Springer International Publishing, Cham, 2014.
- [9] C. Olah, A. Satyanarayan, I. Johnson, S. Carter, L. Schubert, K. Ye, and A. Mordvintsev, “The building blocks of interpretability,”
- [10] A. Ansuini, A. Laio, J. H. Macke, and D. Zoccolan, “Intrinsic dimension of data representations in deep neural networks,” *arXiv [cs.LG]* (May, 2019).
- [11] D. Doimo, A. Glielmo, A. Ansuini, and A. Laio, “Hierarchical nucleation in deep neural networks,” in *Advances in Neural Information Processing Systems*, H. Larochelle, M. Ranzato, R. Hadsell, M. F. Balcan, and H. Lin, eds., vol. 33, pp. 7526–7536. Curran Associates, Inc., 2020.
- [12] P. Pope, C. Zhu, A. Abdelkader, M. Goldblum, and T. Goldstein, “The intrinsic dimension of images and its impact on learning,” *arXiv preprint arXiv:2104.08894* (2021).
- [13] L. Valeriani, D. Doimo, F. Cuturello, A. Laio, A. Ansuini, and A. Cazzaniga, “The geometry of hidden representations of large transformer models,” in *Advances in Neural Information Processing Systems*, A. Oh, T. Naumann, A. Globerson, K. Saenko, M. Hardt, and S. Levine, eds., vol. 36, pp. 51234–51252. Curran Associates, Inc., 2023. [https://proceedings.neurips.cc/paper\\_files/paper/2023/file/a0e66093d7168b40246af1cddc025daa-Paper-Conference.pdf](https://proceedings.neurips.cc/paper_files/paper/2023/file/a0e66093d7168b40246af1cddc025daa-Paper-Conference.pdf).
- [14] E. Tulchinskii, K. Kuznetsov, L. Kushnareva, D. Cherniavskii, S. Barannikov, I. Piontkovskaya, S. Nikolenko, and E. Burnaev, “Intrinsic dimension estimation for robust detection of AI-generated texts,” *arXiv [cs.CL]* (June, 2023).
- [15] E. Cheng, C. Kervadec, and M. Baroni, “Bridging information-theoretic and geometric compression in language models,” in *Proceedings of the 2023 Conference on Empirical Methods in Natural Language Processing*, H. Bouamor, J. Pino, and K. Bali, eds., pp. 12397–12420. Association for Computational Linguistics, Singapore, Dec., 2023. <https://aclanthology.org/2023.emnlp-main.762>.
- [16] S. Mandal, A. Guzmán-Sáenz, N. Haiminen, S. Basu, and L. Parida, “A topological data analysis approach on predicting phenotypes from gene expression data,” in *Algorithms for Computational Biology*, C. Martín-Vide, M. A. Vega-Rodríguez, and T. Wheeler, eds., pp. 178–187. Springer International Publishing, Cham, 2020.
- [17] M. Biagetti, A. Cole, and G. Shiu, “The persistence of large scale structures. part i. primordial non-gaussianity,” *Journal of Cosmology and Astroparticle Physics* **2021** no. 04, (Apr., 2021) 061. <http://dx.doi.org/10.1088/1475-7516/2021/04/061>.
- [18] J. H. T. Yip, M. Biagetti, A. Cole, K. Viswanathan, and G. Shiu, “Cosmology with persistent homology: a Fisher forecast,” *JCAP* **09** (2024) 034, arXiv:2403.13985 [astro-ph.CO].
- [19] Y. Skaf and R. Laubenbacher, “Topological data analysis in biomedicine: A review,” *Journal of Biomedical Informatics* **130** (2022) 104082. <https://www.sciencedirect.com/science/article/pii/S1532046422000983>.
- [20] A. B. El-Yaagoubi, M. K. Chung, and H. Ombao, “Topological data analysis for multivariate time series data,” *Entropy* **25** no. 11, (2023). <https://www.mdpi.com/1099-4300/25/11/1509>.
- [21] F. Hensel, M. Moor, and B. Rieck, “A survey of topological machine learning methods,” *Frontiers in Artificial Intelligence* **4** (2021). <https://www.frontiersin.org/journals/artificial-intelligence/articles/10.3389/frai.2021.681108>.
- [22] Rieck, Bastian Alexander, Togninalli, Matteo, Bock, Christian, Moor, Michael, Horn, Max, Gumbsch, Thomas, and Borgwardt, Karsten, “Neural persistence: A complexity measure for deep neural networks using algebraic topology,” <http://hdl.handle.net/20.500.11850/327207>.
- [23] G. Naitzat, A. Zhitnikov, and L.-H. Lim, “Topology of deep neural networks,” 2020. <https://arxiv.org/abs/2004.06093>.
- [24] G. Magai and A. Ayzenberg, “Topology and geometry of data manifold in deep learning,” *ArXiv abs/2204.08624* (Apr., 2022).
- [25] I. Goodfellow, Y. Bengio, A. Courville, and Y. Bengio, *Deep learning*, vol. 1. MIT Press, 2016.
- [26] A. Rathore, N. Chalapathi, S. Palande, and B. Wang, “TopoAct: Visually exploring the shape of activations in deep learning,” *arXiv [cs.CG]* (Dec., 2019).

- [27] S. Barannikov, I. Trofimov, N. Balabin, and E. Burnaev, “Representation topology divergence: A method for comparing neural network representations.” in *Proceedings of the 39th International Conference on Machine Learning*, K. Chaudhuri, S. Jegelka, L. Song, C. Szepesvari, G. Niu, and S. Sabato, eds., vol. 162 of *Proceedings of Machine Learning Research*, pp. 1607–1626. PMLR, 17–23 jul, 2022. <https://proceedings.mlr.press/v162/barannikov22a.html>.
- [28] S. Suresh, B. Das, V. Abrol, and S. D. Roy, “On characterizing the evolution of embedding space of neural networks using algebraic topology,” *arXiv [cs.LG]* (Nov., 2023) .
- [29] G. Carlsson and V. de Silva, “Zigzag persistence,” *Found. Comput. Math.* **10** no. 4, (Aug., 2010) 367–405.
- [30] G. E. Carlsson, V. de Silva, and D. Morozov, “Zigzag persistent homology and real-valued functions,” in *SCG '09*. 2009. <https://api.semanticscholar.org/CorpusID:5801261>.
- [31] A. Tausz and G. E. Carlsson, “Applications of zigzag persistence to topological data analysis,” *CoRR abs/1108.3545* (2011), 1108.3545. <http://arxiv.org/abs/1108.3545>.
- [32] S. Tymochko, E. Munch, and F. A. Khasawneh, “Using zigzag persistent homology to detect hopf bifurcations in dynamical systems,” *Algorithms* **13** no. 11, (Oct., 2020) 278. <http://dx.doi.org/10.3390/a13110278>.
- [33] A. Myers, D. Muñoz, F. A. Khasawneh, and E. Munch, “Temporal network analysis using zigzag persistence,” *EPJ Data Science* **12** no. 1, (2023) 6.
- [34] R. McDonald, R. Neuhausler, M. Robinson, L. Larsen, H. Harrington, and M. Bruna, “Zigzag persistence for coral reef resilience using a stochastic spatial model,” *Journal of the Royal Society, Interface* **20** (08, 2023) 20230280.
- [35] J. Yang, H. Fang, J. Dhesi, I. H. Yoon, J. A. Bull, H. M. Byrne, H. A. Harrington, and G. Grindstaff, “Topological classification of tumour-immune interactions and dynamics,” *arXiv preprint arXiv:2308.05294* (2023) .
- [36] M. Zhang, S. Chowdhury, and M. Saggat, “Temporal mapper: Transition networks in simulated and real neural dynamics,” *Network Neuroscience* **7** no. 2, (2023) 431–460.
- [37] G. Gharooni-Fard, M. Byers, V. Deshmukh, E. Bradley, C. Mayo, C. M. Topaz, and O. Peleg, “A computational topology-based spatiotemporal analysis technique for honeybee aggregation,” *npj Complexity* **1** no. 1, (2024) 3.
- [38] W. Kim and F. Mémoli, “Spatiotemporal persistent homology for dynamic metric spaces,” *Discrete & Computational Geometry* **66** (2021) 831–875.
- [39] L. Xian, H. Adams, C. M. Topaz, and L. Ziegelmeier, “Capturing dynamics of time-varying data via topology,” *arXiv [cs.LG]* (Oct., 2020) .
- [40] A. Fan, E. Grave, and A. Joulin, “Reducing transformer depth on demand with structured dropout,” in *International Conference on Learning Representations*. 2020. <https://openreview.net/forum?id=Sy1O2yStDr>.
- [41] M. Zhang and Y. He, “Accelerating training of transformer-based language models with progressive layer dropping,” in *Advances in Neural Information Processing Systems*, H. Larochelle, M. Ranzato, R. Hadsell, M. Balcan, and H. Lin, eds., vol. 33, pp. 14011–14023. Curran Associates, Inc., 2020. [https://proceedings.neurips.cc/paper\\_files/paper/2020/file/all140a3d0df1c81e24ae954d935e8926-Paper.pdf](https://proceedings.neurips.cc/paper_files/paper/2020/file/all140a3d0df1c81e24ae954d935e8926-Paper.pdf).
- [42] C. Fan, J. Li, X. Ao, F. Wu, Y. Meng, and X. Sun, “Layer-wise model pruning based on mutual information,” *arXiv preprint arXiv:2108.12594* (2021) .
- [43] A. H. Jha, T. Sherborne, E. P. Walsh, D. Groeneveld, E. Strubell, and I. Beltagy, “Just chop: Embarrassingly simple llm compression,” 2024. <https://arxiv.org/abs/2305.14864>.
- [44] H. Sajjad, F. Dalvi, N. Durrani, and P. Nakov, “On the effect of dropping layers of pre-trained transformer models,” *Comput. Speech Lang.* **77** no. C, (Jan., 2023) . <https://doi.org/10.1016/j.csl.2022.101429>.
- [45] S. A. Siddiqui, X. Dong, G. Heinrich, T. Breuel, J. Kautz, D. Krueger, and P. Molchanov, “A deeper look at depth pruning of llms,” 2024. <https://arxiv.org/abs/2407.16286>.
- [46] S. He, G. Sun, Z. Shen, and A. Li, “What matters in transformers? not all attention is needed,” 2024. <https://arxiv.org/abs/2406.15786>.
- [47] Y. Zhang, Y. Dong, and K. Kawaguchi, “Investigating layer importance in large language models,” 2024. <https://arxiv.org/abs/2409.14381>.

- [48] B.-K. Kim, G. Kim, T.-H. Kim, T. Castells, S. Choi, J. Shin, and H.-K. Song, “Shortened llama: Depth pruning for large language models with comparison of retraining methods,” 2024. <https://arxiv.org/abs/2402.02834>.
- [49] Y. Zhang, Y. Li, X. Wang, Q. Shen, B. Plank, B. Bischl, M. Rezaei, and K. Kawaguchi, “Finer-cut: Finer-grained interpretable layer pruning for large language models,” 2024. <https://arxiv.org/abs/2405.18218>.
- [50] M. Klabunde, T. Schumacher, M. Strohmaier, and F. Lemmerich, “Similarity of neural network models: A survey of functional and representational measures,” *arXiv preprint arXiv:2305.06329* (2023).
- [51] Edelsbrunner, Letscher, and Zomorodian, “Topological persistence and simplification,” *Discrete & computational geometry* **28** (2002) 511–533.
- [52] A. Zomorodian and G. Carlsson, “Computing persistent homology,” in *Proceedings of the twentieth annual symposium on Computational geometry*, pp. 347–356. 2004.
- [53] G. Carlsson, “Topology and data,” *Bulletin of the American Mathematical Society* **46** no. 2, (2009) 255–308.
- [54] D. Morozov, “Dionysus2.” <https://www.mrzv.org/software/dionysus2/>.
- [55] T. K. Dey and T. Hou, “Fast computation of zigzag persistence,” 2022. <https://arxiv.org/abs/2204.11080>.
- [56] W. Kim and F. Mémoli, “Stable signatures for dynamic graphs and dynamic metric spaces via zigzag persistence,” *arXiv: Algebraic Topology* (2017). <https://api.semanticscholar.org/CorpusID:44017453>.
- [57] H. Touvron, L. Martin, K. Stone, P. Albert, A. Almahairi, Y. Babaei, N. Bashlykov, S. Batra, P. Bhargava, S. Bhosale, D. Bikel, L. Blecher, C. C. Ferrer, M. Chen, G. Cucurull, D. Esiobu, J. Fernandes, J. Fu, W. Fu, B. Fuller, C. Gao, V. Goswami, N. Goyal, A. Hartshorn, S. Hosseini, R. Hou, H. Inan, M. Kardas, V. Kerkez, M. Khabsa, I. Kloumann, A. Korenev, P. S. Koura, M.-A. Lachaux, T. Lavril, J. Lee, D. Liskovich, Y. Lu, Y. Mao, X. Martinet, T. Mihaylov, P. Mishra, I. Molybog, Y. Nie, A. Poulton, J. Reizenstein, R. Rungta, K. Saladi, A. Schelten, R. Silva, E. M. Smith, R. Subramanian, X. E. Tan, B. Tang, R. Taylor, A. Williams, J. X. Kuan, P. Xu, Z. Yan, I. Zarov, Y. Zhang, A. Fan, M. Kambadur, S. Narang, A. Rodriguez, R. Stojnic, S. Edunov, and T. Scialom, “Llama 2: Open foundation and fine-tuned chat models,” 2023. <https://arxiv.org/abs/2307.09288>.
- [58] AI@Meta, “Llama 3 model card,” [https://github.com/meta-llama/llama3/blob/main/MODEL\\_CARD.md](https://github.com/meta-llama/llama3/blob/main/MODEL_CARD.md).
- [59] A. Q. Jiang, A. Sablayrolles, A. Mensch, C. Bamford, D. S. Chaplot, D. de las Casas, F. Bressand, G. Lengyel, G. Lample, L. Saulnier, L. R. Lavaud, M.-A. Lachaux, P. Stock, T. L. Scao, T. Lavril, T. Wang, T. Lacroix, and W. E. Sayed, “Mistral 7b,” 2023. <https://arxiv.org/abs/2310.06825>.
- [60] S. Biderman, H. Schoelkopf, Q. Anthony, H. Bradley, K. O’Brien, E. Hallahan, M. A. Khan, S. Purohit, U. S. Prashanth, E. Raff, A. Skowron, L. Sutawika, and O. van der Wal, “Pythia: A suite for analyzing large language models across training and scaling,” 2023. <https://arxiv.org/abs/2304.01373>.
- [61] L. Gao, S. Biderman, S. Black, L. Golding, T. Hoppe, C. Foster, J. Phang, H. He, A. Thite, N. Nabeshima, S. Presser, and C. Leahy, “The Pile: An 800gb dataset of diverse text for language modeling,” *arXiv preprint arXiv:2101.00027* (2020).
- [62] R. Socher, A. Perelygin, J. Wu, J. Chuang, C. D. Manning, A. Ng, and C. Potts, “Recursive deep models for semantic compositionality over a sentiment treebank,” in *Proceedings of the 2013 Conference on Empirical Methods in Natural Language Processing*, pp. 1631–1642. Association for Computational Linguistics, Seattle, Washington, USA, Oct., 2013. <https://www.aclweb.org/anthology/D13-1170>.
- [63] D. Hendrycks, C. Burns, S. Basart, A. Zou, M. Mazeika, D. Song, and J. Steinhardt, “Measuring massive multitask language understanding,” *Proceedings of the International Conference on Learning Representations (ICLR)* (2021).
- [64] R. Zellers, A. Holtzman, Y. Bisk, A. Farhadi, and Y. Choi, “HellaSwag: Can a machine really finish your sentence?,” in *Proceedings of the 57th Annual Meeting of the Association for Computational Linguistics*, A. Korhonen, D. Traum, and L. Márquez, eds., pp. 4791–4800. Association for Computational Linguistics, Florence, Italy, July, 2019. <https://aclanthology.org/P19-1472>.
- [65] K. Sakaguchi, R. L. Bras, C. Bhagavatula, and Y. Choi, “Winogrande: An adversarial winograd schema challenge at scale,” 2019. <https://arxiv.org/abs/1907.10641>.

- [66] L. Gao, J. Tow, B. Abbasi, S. Biderman, S. Black, A. DiPofi, C. Foster, L. Golding, J. Hsu, A. Le Noac’h, H. Li, K. McDonnell, N. Muennighoff, C. Ociepa, J. Phang, L. Reynolds, H. Schoelkopf, A. Skowron, L. Sutawika, E. Tang, A. Thite, B. Wang, K. Wang, and A. Zou, “A framework for few-shot language model evaluation,” 07, 2024. <https://zenodo.org/records/12608602>.
- [67] P. Gabriel, “Unzerlegbare darstellungen i,” *manuscripta mathematica* **6** no. 1, (Mar., 1972) 71–103. <http://dx.doi.org/10.1007/BF01298413>.

## A Mathematical Formulation of Zig Zag Persistence

Zigzag persistence is a computational topology method that extends classical persistent homology to handle more complex data structures and filtration processes. Unlike standard persistence, which analyzes a single sequence of spaces filtered by inclusion, zigzag persistence allows for the exploration of data where sequences of spaces and maps can move both forward and backward.

A *zigzag filtration* of topological spaces is a sequence:

$$\chi: \mathbb{X}_1 \longleftrightarrow \mathbb{X}_2 \longleftrightarrow \cdots \longleftrightarrow \mathbb{X}_{n-1} \longleftrightarrow \mathbb{X}_n, \quad (7)$$

where each  $\mathbb{X}_i$  is a topological space and each arrow  $\longleftrightarrow$  represents a continuous function pointing forwards  $\mathbb{X}_i \rightarrow \mathbb{X}_{i+1}$  or backwards  $\mathbb{X}_i \leftarrow \mathbb{X}_{i+1}$ .

If we apply a homology functor  $H_p$  with coefficients in a field  $\mathbf{k}$  to such a filtration, we get a zigzag filtration of  $\mathbf{k}$ -vector spaces, called *zigzag module*:

$$H_p(\chi): H_p(\mathbb{X}_1) \longleftrightarrow H_p(\mathbb{X}_2) \longleftrightarrow \cdots \longleftrightarrow H_p(\mathbb{X}_{n-1}) \longleftrightarrow H_p(\mathbb{X}_n). \quad (8)$$

It is proven in [29] that the algebraic classification of zigzag modules resembles Gabriel’s classification of the persistence module described in [67]. In particular, every finite-dimensional zigzag module, i.e. for which all the  $\mathbf{k}$ -vector spaces in the sequence that are finite-dimensional, can be decomposed as a direct sum of interval modules, where a (finitely indexed) *interval module* is a module of the form:

$$\mathcal{I}_{[b,d]}: I_1 \longleftrightarrow I_2 \longleftrightarrow \cdots \longleftrightarrow I_n, \quad (9)$$

where  $I_i = \mathbf{k}$  for  $b \leq i \leq d$ , and  $I_i = 0$  otherwise, and every arrow of the form  $\mathbf{k} \leftarrow \mathbf{k}$  or  $\mathbf{k} \rightarrow \mathbf{k}$  is the identity map. Moreover, the list of summands is unique up to reordering.

The *zigzag persistence diagram* of a filtration  $\chi$  in dimension  $p$  is the multiset of intervals  $[b, d]$  corresponding to the list of interval summands  $\mathcal{I}_{[b,d]}$  of  $H_p(\chi)$ . In other words,

$$\text{Pers}_p(\chi) = \{[b_j, d_j] : j \in J\} \iff H_p(\chi) \cong \bigoplus_{j \in J} \mathcal{I}_{[b_j, d_j]} \quad (10)$$

Each interval  $[b, d]$  is called *persistence interval* and is thought of as a persistent homological feature of  $\chi$  that appears at time  $b$  (referred to as the “birth”) and disappears at time  $d$  (referred to as the “death”).

In our approach, the use of intersection layers is essential for computing zigzag persistence, as it allows the construction of injective maps between the  $k_{\text{NN}}$  complexes of model layers (see equation 2)<sup>10</sup>. Since our primary goal is to analyze the topological changes between model layers, we eliminate the construction of intersection layers while preserving the topological features by shifting each persistence interval such that the birth and death times occur strictly within the layers.

For an interval  $[b, d]$  in the zigzag persistence diagram of dimension  $p$  of filtration 2, the mapping that enables a bijective transformation to a new interval  $[\hat{b}, \hat{d}]$ <sup>11</sup> only across model layers is defined as follows:

$$\hat{b} = \begin{cases} b + 1 & \text{if } b \text{ is an intersection layer} \\ b & \text{otherwise} \end{cases}, \quad \hat{d} = \begin{cases} d + 1 & \text{if } d \text{ is an intersection layer} \\ d & \text{otherwise} \end{cases} \quad (11)$$

<sup>9</sup>In our setting we say a  $p$ -cycle “dies”, we mean that the corresponding homology class no longer persists in subsequent layers. In the zigzag filtration, this happens when the cycle is no longer represented by an independent equivalence class in the homology group.

<sup>10</sup>An alternative method for constructing these maps and obtaining the zigzag persistence diagram is to use a filtration where, instead of intersections, the union of the complexes from two consecutive layers is considered. However, the Diamond Lemma, as discussed in [30], guarantees that both the intersection- and union-based filtrations encode the same homological information.

<sup>11</sup>By construction, all resulting intervals contain even numbers, as the model layers are indexed with these numbers.

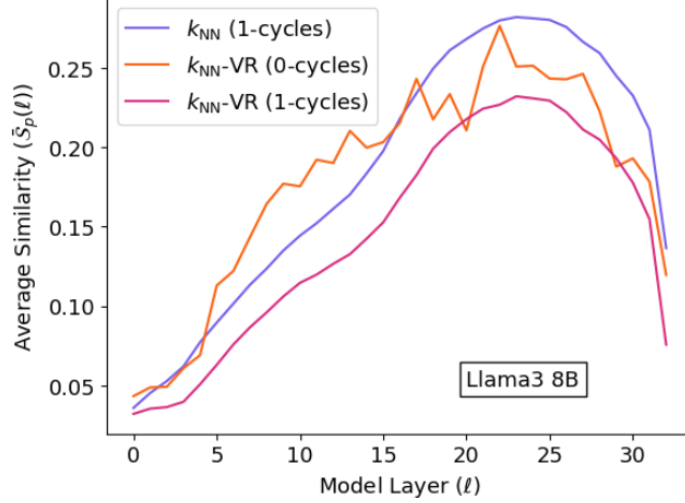


Figure 6: Plot of the Average Similarity as a function of model layers computed for Llama3 8B for both  $k_{NN}$  and  $k_{NN}$ -VR complexes. We impose the number of 0-cycles,  $\beta_0 = 500 \pm 100$  to build the  $k_{NN}$ -VR complexes.

The relationship between the persistence image and the effective persistence image for  $p$ -cycles, denoted respectively by  $PI_p$  and  $\widehat{PI}_p$ , where  $b, d$  are the model layers indexed by even numbers, is described by the following system of equations:

$$\begin{cases} \widehat{PI}_p(0, 0) = PI_p(0, 0) \\ \widehat{PI}_p(b/2, d/2) = PI_p(b, d) + PI_p(b-1, d) + PI_p(b, d-1) + PI_p(b-1, d-1) \\ \widehat{PI}_p(b/2, \infty) = PI_p(b, \infty) + PI_p(b-1, \infty). \end{cases} \quad (12)$$

## B Combining the $k_{NN}$ graph with the Vietoris-Rips complex

The  $k$ -nearest neighbors ( $k_{NN}$ ) complex is built by expanding the corresponding  $k_{NN}$  graph to a fixed dimension  $m$ . A key limitation of the  $k_{NN}$  complex is that it ranks points by proximity without considering their actual distances. As a result, once  $k$  is fixed on each layer, each point is connected to its  $k$ -nearest neighbors, regardless of the absolute distances involved. In our setting, the number of 0-cycles (the Betti <sup>12</sup> number  $\beta_0$ ) of the  $k_{NN}$  complexes as a function of the layers tends to be unity, i.e. the whole complex is connected, even for relatively small values of  $k_{NN} \gtrsim 6$ . This implies that 0-cycles contain no useful topological information on the internal representations.

To address this issue, we follow the approach in [23], which combines the  $k_{NN}$  complex with the Vietoris-Rips complex. Starting from the  $k_{NN}$  graph, the idea is to introduce a threshold radius  $R$  on each layer and use it to filter out edges of the graph whose lengths are less than or equal to  $R$ , and then expand, denoting this new complex  $k_{NN}$ -VR. This filtering step allows us to focus on longer-range connections, uncovering significant topological features that may be hidden by shorter, more local connections.

To ensure consistency across layers, we select the radius  $R$  in each layer such that the number of 0-cycles,  $\beta_0$ , of the  $k_{NN}$  complex falls in a pre-determined range. We then compute the observables presented in this work and verify the results. For clarity, we refer to  $k_{NN}$  complex the construction used in the main body, and  $k_{NN}$ -VR complexes the one presented in this section. For the sake of conciseness, we present only results for the average similarity  $\bar{S}$ . In Figure 6 we show the average similarity of 1-cycles of the  $k_{NN}$  and the  $k_{NN}$ -VR complexes and the 0-cycles of the  $k_{NN}$ -VR complexes computed by imposing  $\beta_0 = 500 \pm 100$ . <sup>13</sup> We observe all three curves are qualitatively and quantitatively similar. This indicates that information about the similarity of 1-cycles remains unchanged, even when removing a considerable amount of short edges. Moreover, we observe the same information also on 0-cycles, now that we modified the complex such that their statistics are large enough to reliably compute similarity. We argue this

<sup>12</sup>Betti numbers have been used in previous works [23, 28] for interpreting internal representations of neural networks. However, they describe each layer independently from the others, which is not the purpose of this work.

<sup>13</sup>We checked that results are consistent as long as  $\beta_0$  is much lower than the total number of points.

indicates a universal (in homology) tendency to retain relational connections among particles in the middle-late layers of the model.

## C Consistency of Results

### C.1 Average Similarity on Pile

To show the consistency of our method, we computed our observables on both representations from the Pile-10K dataset and SST dataset. For Pile-10K, we did not compute them on the largest models of 70B parameters to reduce computational usage. Nevertheless, we show here the effective persistence image, persistence similarity and average similarity in Figure 7.

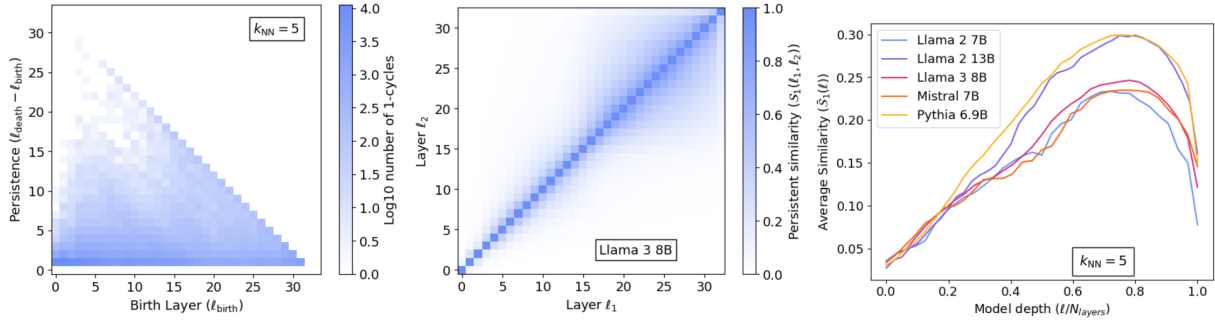


Figure 7: Effective persistence image (left), persistence similarity (middle) and average similarity (right) for the Pile-10K dataset.